

Quench dynamics across the MI-SF quantum phase transition with cluster mean field theory

Deepak Gaur,^{1,2} Hrushikesh Sable,^{1,3} and D. Angom⁴

¹*Physical Research Laboratory, Ahmedabad - 380009, Gujarat, India*

²*Indian Institute of Technology Gandhinagar, Palaj, Gandhinagar - 382355, Gujarat, India*

³*Department of Physics, Virginia Tech, Blacksburg, Virginia 24061, USA*

⁴*Department of Physics, Manipur University, Canchipur - 795003, Manipur, India*

In this work, we study the quench dynamics of quantum phases of ultracold neutral bosons trapped in optical lattices. We investigate the validity of the Kibble-Zurek (KZ) scaling laws with the single-site Gutzwiller mean-field (SGMF) and cluster Gutzwiller mean-field (CGMF) theory. With CGMF, we note the evolution of the dynamical wavefunction in the “impulse” regime of the Kibble-Zurek mechanism. We obtain the power law scalings for the crossover time and defect density with the quench rate predicted by KZ scaling laws. The critical exponents obtained from dynamics are close to their equilibrium values. Furthermore, it is observed that the obtained dynamical critical exponent z improves towards the equilibrium value with increasing cluster sizes in CGMF.

I. INTRODUCTION

The non-equilibrium phenomena involving a quench across a continuous phase transition follow universal scalings relations given in terms of the equilibrium critical exponents, as explained by the Kibble-Zurek Mechanism (KZM) [1–4]. The KZM is based on the idea of critical slowing down near the continuous phase transition. As a result, the system is no longer able to catch up the change in the parameters, however slow the change in parameters be, and the adiabaticity breaks down. The spontaneous symmetry breaking at the phase transition would then lead to topological defects in the system due to independent local choices of symmetry breaking in different parts of the system. KZM assumes the temporal evolution of the state as adiabatic far from the critical point and assumes it as an impulse when the system parameters are sufficiently close to the critical point of phase transition. After the critical point is passed and the system parameters are sufficiently away, the adiabaticity is finally restored. With this, the KZM predicts the density of the topological defects to follow a power law scaling with the quench rate, and the scaling exponents are given in terms of the equilibrium critical exponents of the phase transition. In Condensed matter systems, the KZM started with the works of Zurek, and the prediction of the scaling laws for the correlation length and defect density was afterward experimentally verified in superfluid helium [1, 5–7]. Later on, the KZM was applied to classical phase transitions in a variety of condensed matter systems and eventually to quantum phase transitions (QPTs) [2, 4, 8].

Ultracold neutral bosonic atoms in optical lattices are excellent systems for studying quantum phases and the QPTs and quantum phases in the laboratory. This engineered system is used as a macroscopic quantum simulator for a variety of condensed matter systems [9, 10]. We investigate the quench dynamics of the quantum phase supported by the system of ultracold neutral bosons in optical lattices described by the Bose-Hubbard model (BHM). The ground state of the BHM Hamiltonian consists of the incompressible Mott-insulator (MI) and compressible superfluid (SF) states as the quantum phases [11, 12]. The BHM shows a QPT between the MI and SF phases at the critical value of the model parameters [13, 14].

We have studied the KZM scaling laws for MI-SF QPT by evolving the MI state under a quantum quench, taking the system across the phase transition into the SF regime. Various experimental works exist on the quench dynamics across the MI-SF QPT and KZ scaling [15, 16]. On the theoretical side, there are studies investigating the KZM for QPTs in BHM and its extensions [17–24]. However, the dynamically obtained exponents differ from the equilibrium critical exponents. In this work, we explore the KZM scaling laws with the SGMF method and compare it with the CGMF study to see the effect due to intra-cluster dynamics, which is captured exactly compared to the single-site mean-field description. The CGMF also allows better relaxation dynamics due to a large Fock-state space. We have chosen to study the QPT at fixed chemical potential $\mu = 0.3U$, which corresponds to a first-order phase transition, and also at the tip of the Mott-1 lobe at $\mu = 0.4U$, which corresponds to a continuous phase transition and belongs to the 3D XY model universality class. The quench is performed by increasing the hopping strength. For MI-SF QPT, the equilibrium critical exponents have the values of the 3D XY model at the tip of the Mott lobe $\nu = 2/3$ and $z = 1$, and away from the tip, the exponents have mean-field values $\nu = 1/2$ and $z = 2$ [11]. In our study, we observe the power-law scalings as predicted by KZM and find that the dynamically obtained critical exponents deviate from their equilibrium values. However, the mismatch for the critical exponent associated with the divergence of relaxation time reduces with the CGMF study. The CGMF study captures the evolution in the quenched state in the “impulse” regime of KZM against the assumption of frozen dynamics. This dynamics is absent in the SGMF studies. The frozen state dynamics in the impulse regime have been explored in various works [25–27]. The many-body localization, thermalization, and entanglement dynamics following the quench are various other research pursuits explored using the quantum quenches [28, 29].

We have organized the remainder of this article as follows. In Sec. II, we describe the BHM model, which describes the system. Here, we also give a brief discussion of the numerical mean-field methods used by us and a brief discussion of KZM. This is followed by the results from the quench dynamics study, which is discussed in Sec. III. We first discuss the

quench dynamics across the QPT below the tip of the Mott lobe. Here, we discuss the findings from SGMF and CGMF studies and compare them. At the end, we discuss the quench across the QPT at the tip of the Mott lobe. Finally, we summarize and conclude the findings in Sec.IV

II. THEORY

Consider a system of bosonic atoms loaded in a 2D square optical lattice. The system is well described by the Bose-Hubbard model and the Hamiltonian of the system is [12]

$$\hat{H} = \sum_{p,q} \left[-\left(J\hat{b}_{p+1,q}^\dagger \hat{b}_{p,q} + J\hat{b}_{p,q+1}^\dagger \hat{b}_{p,q} + \text{H.c.} \right) + \frac{U}{2} \hat{n}_{p,q} (\hat{n}_{p,q} - 1) - \mu \hat{n}_{p,q} \right] \quad (1)$$

where p (q) is the lattice site index along the x (y) direction, $\hat{b}_{p,q}$ ($\hat{b}_{p,q}^\dagger$) is the annihilation (creation) operator at the lattice site (p, q) , $\hat{n}_{p,q}$ is the number operator, and U is the on-site interaction strength. The chemical potential μ fixes the total number of particles in the system and is suitable for studies with a mean-field in the grand-canonical ensemble. The ground state of the system can be obtained using the mean-field methods which decouples the bi-linear operators of neighboring lattice sites in the hopping term.

A. Mean-field methods

In the SGMF method, the annihilation and creation operators are decomposed in terms of a mean field and a fluctuation operator as $\hat{b}_{p,q} = \phi_{p,q} + \delta\hat{b}_{p,q}$ [30, 31]. Here $\phi_{p,q} = \langle \hat{b}_{p,q} \rangle$ is the mean-field and given by the expectation value of the annihilation operator with respect to the ground state of the system. This approximation allows the mean-field Hamiltonian of the system to be written as a direct sum of the mean-field Hamiltonians of the single sites

$$\hat{h}_{p,q} = -\left(J\phi_{p+1,q}^* \hat{b}_{p,q} + J\phi_{p,q+1}^* \hat{b}_{p,q} + \text{H.c.} \right) + \frac{U}{2} \hat{n}_{p,q} (\hat{n}_{p,q} - 1) - \mu \hat{n}_{p,q}. \quad (2)$$

The ground state wavefunction can be expressed a product of the wavefunctions at each of the lattice sites by employing the Gutzwiller ansatz

$$|\Psi\rangle_{GW} = \prod_{p,q} |\psi\rangle_{p,q} = \prod_{p,q} \sum_{n=0}^{N_b} c_n^{p,q} |n\rangle_{p,q}. \quad (3)$$

Here, $|n\rangle_{p,q}$ forms the Fock-space basis with N_b representing the maximum allowed occupation number, and $c_n^{p,q}$ s are the coefficients of the basis state $|n\rangle_{p,q}$.

To better account the correlation effects in the system, the CGMF method is used. In this method the lattice is tiled with

clusters and for the hopping within the same cluster or intra-cluster hopping, the hopping term of the BHM Hamiltonian is calculated exactly. However, inter-cluster hopping is calculated using the mean-field. Like in the case of SGMF, the Hamiltonian of the system can be written as a direct sum of the cluster Hamiltonians and the mean field terms which couple the clusters [32]. The ground state Gutzwiller wavefunction can then be defined as the direct product of cluster wavefunctions expressed in the coupled basis. For the cluster of size $M \times N$, the cluster wavefunction is

$$|\psi_c\rangle = \sum_{n_1, n_2, \dots, n_{MN}} C_{n_1, n_2, \dots, n_{MN}} |n_1, n_2, \dots, n_{MN}\rangle, \quad (4)$$

where n_1, n_2, \dots, n_{MN} are the occupancies at the sites within the cluster which are labelled with indices $1, 2, \dots, MN$. The equilibrium ground state is obtained numerically in a self-consistent iterative process. Starting with a random initial guess state, the Hamiltonian matrix is constructed and diagonalized to obtain the ground state wavefunction. From this wavefunction the mean-field is calculated which is then used as an improved guess. The iterations are performed till the mean-field converges [33, 34].

The dynamics of the initial equilibrium state is studied by temporal evolution of the wavefunction according to the time-dependent Gutzwiller equations. These equations are essentially the Euler-Lagrange equations of motion derived from the Lagrangian of the system. The time-dependent Gutzwiller equations form a set of coupled partial-differential equations in terms of the dynamical coefficients of the wavefunction. These set of equations are solved using the fourth order Runge-Kutta (RK4) method.

B. KZ Scaling for MI-SF QPT

For a quantum quench across the MI-SF QPT, we choose an initial state in the MI regime and quench the tunneling strength J in time till it enters the SF phase domain. The quench protocol is chosen as linear and is given by

$$J(t) = J_i + (J_c - J_i) \frac{t + \tau_Q}{\tau_Q}. \quad (5)$$

Here J_i and J_c are the values of the quench parameter at the beginning of the quench and at the critical point of the MI-SF phase boundary. The different quench rates are realised by different values of the constant τ_Q . Here, we have set $U = 1$ and all system parameters are measured in this unit. The initial MI state evolves in response to the quench in parameter $J(t)$ across the criticality and enters into the Superfluid phase regime. The time instant at which the dynamically evolving state becomes a superfluid state is marked as time \hat{t} and this happens after $t = 0$ corresponding to the criticality J_c . This can be understood from the KZM according to which the critical slowing down near the continuous phase transition results in non-adiabatic evolution under the quench in the neighborhood of the critical point. In the KZM, the evolution of the state is adiabatic far from the criticality and impulse around the critical point. The adiabatic to impulse crossover

time \hat{t} is assumed to be the instant when the system relaxation time equals the inverse transition rate [4]. The power-law divergence of the equilibrium correlation length and relaxation time gives the KZM scaling laws for the defect density at the crossover time in terms of the critical exponents. The crossover time \hat{t} scales as a power law with the quench rate τ_Q and is given by

$$\hat{t} \propto \tau_Q^{\frac{\nu z}{1+\nu z}}. \quad (6)$$

Here, ν and z are the equilibrium critical exponents. The defect density at time \hat{t} also scales as a power law

$$\hat{N}_v \propto \tau_Q^{-\frac{(D-\text{def})\nu}{1+\nu z}}, \quad (7)$$

where, D is the system dimension and def is the dimension of the defects.

The superfluid state is characterised by the non-zero value of the average SF order parameter

$$\phi = \frac{1}{N_s} \sum_{p,q} |\phi_{p,q}|, \quad (8)$$

where, N_s is the total number of lattice sites. Around the crossover time, the system enters in SF phase and ϕ starts growing. The spontaneous symmetry breaking at the phase transition, related to the global U(1) symmetry breaking, leads to the production of topological defects in the system. This arises because of the local choices of the order parameter when the symmetry breaking occurs at the phase transition. This results in the quenched state in the SF phase having numerous topological defects. For the case of point defects, vortex or antivortex, the conservation of angular momentum implies the creation of vortex and anti-vortex occurs in pairs. By definition, the vorticity around a vortex and anti-vortex are +1 and -1, respectively, the total defects in the system can be counted as absolute sum of the vorticity over all the lattice site

$$\begin{aligned} N_v &= \sum_{p,q} |\Omega_{p,q}|, \\ \Omega_{p,q} &= \frac{1}{4} [\sin(\theta_{p+1,q} - \theta_{p,q}) + \sin(\theta_{p+1,q+1} - \theta_{p+1,q}) \\ &\quad - \sin(\theta_{p+1,q+1} - \theta_{p,q+1}) - \sin(\theta_{p,q+1} - \theta_{p,q})], \end{aligned} \quad (9)$$

where $\theta_{p,q}$ is the phase of the SF order parameter $\phi_{p,q}$.

III. RESULTS AND DISCUSSION

We study the quantum quench across the MI-SF phase transition across the MI(1) lobe. As mentioned earlier, we perform a linear quench of the hopping strength J starting from the MI(1) state at $J_i = 0$ as the initial state and quench it across the MI-SF phase boundary into the SF regime. We study the dependence of the cross-over time \hat{t} and defect density at \hat{t} on the quench rate. The initial state corresponds to

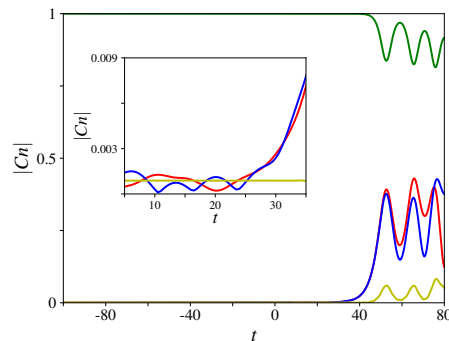


FIG. 1. Dynamical evolution of the absolute magnitude of the coefficients of the basis states with SGMF for $\tau_Q = 100$. Green color curve corresponds to unit filling basis state, red color curve corresponds to the vacuum state, while blue and yellow color curve corresponds to the basis states with two and three particles respectively.

an equilibrium state at J_i . To this equilibrium state, we add small random fluctuations in the wavefunction. This is done to mimic the quantum fluctuations which drives the quantum phase transition. We add random uni-variate phase fluctuation (0 to 2π) in the coefficient of the dominating basis states. Afterwards, we also introduce a random uni-variate density fluctuation of the order 10^{-3} in the coefficients of all the basis states. This completes the preparation of the initial state, and it is then evolved in time. The dynamical state is computed by solving the time-dependent Gutzwiller equations using the RK4 method. The quench is terminated in the superfluid regime. In the RK4 method we choose the time step $\Delta t = 0.005$, and note that the evolution is the same compared with the lower values of $\Delta t = 0.001$. To obtain good statistics of the defects produced during the quench, we choose a large system size of 96×96 and employ the periodic boundary conditions along both the spatial dimensions. The dynamical properties of the state are calculated by taking a sample average of 40 different realizations. We study the quench at constant $\mu = 0.3$ below the tip of the Mott lobe and for $\mu = 0.4$ which corresponds to the tip of the MI(1) lobe. The studies are performed using the SGMF and CGMF methods and the results are discussed below.

A. Quench across QPT below the MI(1) lobe ($\mu = 0.3$)

The initial state is chosen as the MI(1) state on a 96×96 square lattice and is obtained as an equilibrium solution for the system parameters $\mu = 0.3$ and $J = 0$. This initial state is dressed with the fluctuations as mentioned earlier and is then time evolved according to the linear quench protocol. Below we first discuss the properties of the quenched state using the SGMF method, and latter, compare and contrast the findings with the CGMF method.

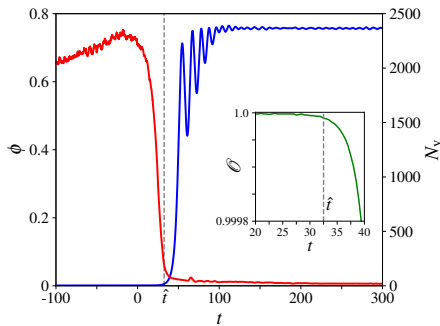


FIG. 2. SF order parameter ϕ (blue) and defect density (red) across the phase transition for $\tau_Q = 100$. After $t = 100$ quench is stopped and the state evolves freely. The crossover time \hat{t} is marked with dashed grey line. The overlap measure \mathcal{O} used to identify the crossover time is shown in the inset.

1. SGMF

The initial MI(1) state at equilibrium is obtained using the SGMF method with a sufficiently large cutoff for the single-site occupancy $N_b = 6$. The Fig.1 shows the temporal evolution of the magnitude of the coefficients of various Fock-states. The green color curve corresponds to the coefficient of $|n = 1\rangle_{p,q}$ Fock state and the red, blue and yellow color curves corresponds to the Fock state with 0, 2 and 3 occupancies respectively. Starting from $t = -\tau_Q$, the adiabatic evolution continues and the quenched state remains in the MI(1) state as can be seen from green curve with value 1. However, the quenched state remains MI(1) state for some time even after crossing the criticality at $t = 0$. This is in agreement with the assumption of impulse regime where the state is frozen. The corresponding fluctuation in the coefficients shown in the plot are of the order of 10^{-3} , which is due to the initial density fluctuations in the dressed state. The quenched state, which is frozen in the impulse domain, starts to evolve dynamically only after the quench parameter J is sufficiently away from J_c . The time evolution of the SF order parameter of the quenched state is shown in Fig.2 for $\tau_Q = 100$. As shown in the figure with blue curve, ϕ is zero initially as it should be in the MI state. However it remains zero even after passing the criticality at $t = 0$ with $J(t = 0) = J_c$, and shows growth only after a certain time instant \hat{t} . After \hat{t} , the SF order parameter grows rapidly and followed by an oscillating trend with decaying amplitude. Finally, after $t = \tau_Q$ when the quench terminates, the system is allowed to evolve freely. In this domain the value of ϕ quickly saturates. The temporal evolution of the defect density (N_v) is shown in Fig.2 with the red curve. At initial times, the system has a large number of vortices and anti-vortices owing to the introduction of phase fluctuations in the initial dressed state. However, N_v decays rapidly after the criticality ($t = 0$) due to the initiation of phase coherence in the system. The KZM scaling laws predicts the power-law scaling of the defect density at \hat{t} with the quench rate. To identify \hat{t} , we use the overlap of the wave-

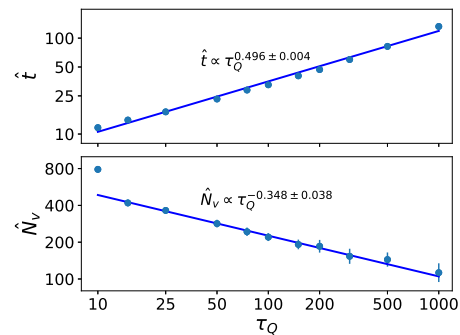


FIG. 3. Power law scaling of \hat{t} and \hat{N}_v with τ_Q . The crossover time is located using the overlap criterion.

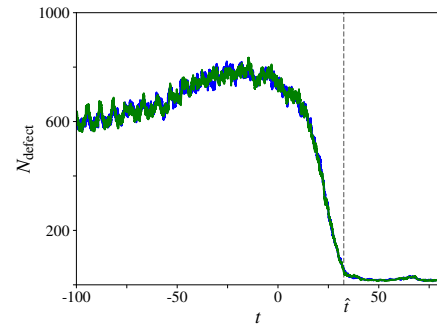


FIG. 4. Plot of topological defects in the quenched state as a function of time. Blue curve shows the number of vortices with a vorticity $\Omega_{p,q} > 0.5$, while the green curve shows the number of anti-vortices with a vorticity $\Omega_{p,q} < -0.5$. The blue and green curves sit on top of each other, with almost equal number of vortex and anti-vortex in the quenched state.

function at any time with the wavefunction at time $t = 0$,

$$\mathcal{O}(t) = |\langle \psi(0) | \psi(t) \rangle|. \quad (10)$$

This definition is motivated from the fact that the dynamical evolution of the state is frozen in the impulse domain as observed in Fig.1. The KZM predicts the overlap to be unity till \hat{t} , and afterwards it can deviate from unity. This is because, in the “impulse” regime the dynamical wavefunction can change with time only upto a phase factor. The deviation of overlap from unity signals the crossing of \hat{t} and occurs when the value of overlap is ≈ 0.99999 . This value depends on the magnitude of the density fluctuations introduced in the dressed initial state. Consequently, we choose a threshold value of 0.99999 for the overlap as a locator of \hat{t} . The overlap measure is shown in the inset of the Fig.2.

For different values of the quench rate τ_Q , we note the crossover time \hat{t} and the corresponding defect density \hat{N}_v , and the results are shown in Fig.3. It can be seen that a power-law scaling exists, but the power-law behaviour shows deviations at the extreme values of quench rates and is much pronounced in the plot of defect density for very fast quenches. However, for very slow quenches, the deviations in the defect density across the samples gives large error bars in the plot. So the

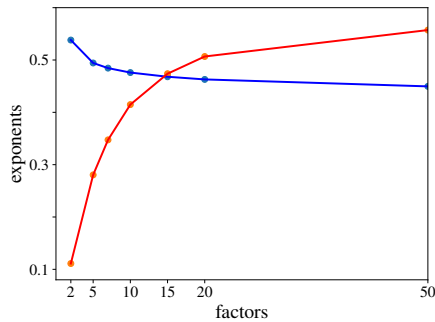


FIG. 5. Scaling exponents for \hat{t} (blue) and \hat{N}_v (red) for various choices of the growth factor $\phi(\hat{t})/\phi(0)$.

power-law exponents are determined by fitting the data points with a power-law in the regime $\tau_Q \in [25, 300]$. From Fig. 3, we note that the crossover time $\hat{t} \propto \tau_Q^{0.496 \pm 0.004}$ and the defect density $\hat{N}_v \propto \tau_Q^{-0.348 \pm 0.038}$. A comparison of these power law exponents with the Eq. 6 and Eq. 7 gives $\nu z/(1 + \nu z) = 0.496 \pm 0.004$ and $(D - \text{def})\nu/(1 + \nu z) = 0.348 \pm 0.038$. A important point to note here is that the topological defects are produced as vortex anti-vortex pairs and constitute as a 1-D defect, that is $\text{def} = 1$ [21]. This can be seen from Fig. 4, where at $t = -\tau_Q$ the initial dressed state have equal number of vortices and anti-vortices owing to the random phase fluctuations. As the quench progresses, the defects are created or annihilated in pairs, thereby maintaining the equality between their numbers. Thus, we obtain the critical exponents $\nu = 0.69 \pm 0.11$ and $z = 1.42 \pm 0.17$.

It should be noted that there are various works in which the crossover time \hat{t} is chosen as the time instant where average SF order parameter becomes twice of its value at criticality $\phi(\hat{t}) = 2\phi(0)$ and around this time ϕ starts to increase rapidly [18, 21]. However, this choice of the growth factor 2 is arbitrary. So, we have also checked the power law scaling for various choices of the growth factor $\phi(\hat{t})/\phi(0)$ and investigated the form of the power law. We find that the variation in the power-law exponents is large and depends on the chosen value of the growth factor. This is reported in Fig. 5 where it can be seen that the variation in the power-law exponents is absent only for large values of the growth factor ~ 20 . This is because around this time, the rate of increase in order parameter is quite large and different choice of the growth factors corresponds to very close values of time t . Comparing this with the overlap criterion discussed earlier, we find that the growth factor of 7 gives reasonably close values for the power-law exponents obtained with the overlap protocol in our studies. Next, we study the dynamics with the CGMF method as described below.

2. CGMF

With the CGMF method, we have chosen 2×2 (and 2×3) clusters to tile the 96×96 lattice. Allowing the single-site occupancy to be almost 2, the coupled basis states for the

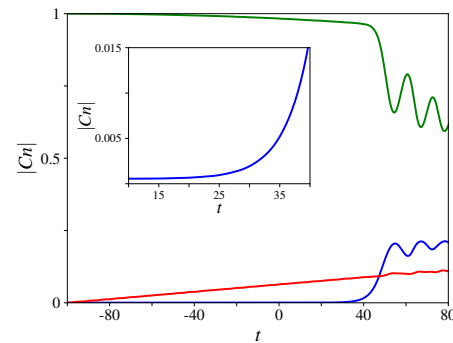


FIG. 6. Dynamical evolution of the absolute magnitude of the coefficients of the basis states with 2×2 cluster CGMF for $\tau_Q = 100$. Green color curve corresponds to uniform unit filling basis state, blue color curve corresponds to the basis state with an extra particle/hole on top of uniform unit filling, and red color curve corresponds to 4-particle states different from uniform unit filling.

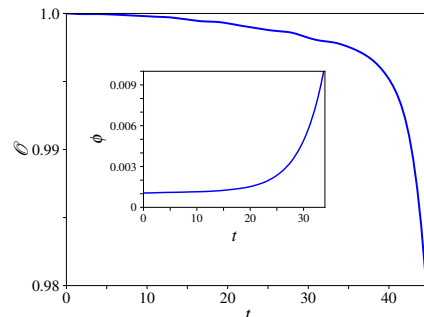


FIG. 7. Overlap measure with 2×2 cluster CGMF for $\tau_Q = 100$. Overlap doesn't show a sharp decay and is not-suitable for locating \hat{t} . The average SF order parameter is shown in the inset.

2×2 cluster now comprise of total 81 possible configurations (729 basis states for 2×3). It is difficult to use large clusters in studying the dynamics as the associated size of the Fock space grow exponentially large with increasing cluster sizes. To circumvent this problem by reduction of basis states appropriately is not a good idea, as in dynamics the excitations are introduced in the state near the phase transition (the extra energy being proportional to the fastness of the quench rate). We have checked this behaviour in our studies. We also observe the intra-cluster dynamics to be present near the critical point which is absent in the SGMF method. This intra-cluster dynamics can be seen in Fig. 6 where the absolute magnitude of the coefficients for some of the basis states are plotted for studies with 2×2 cluster. The red color curve corresponding to the coefficient of basis states with 4 particles but different from the uniformly filled basis state keeps growing from the beginning of quench. And the strength of the uniform unit filling basis state (green color curve) decreases with time. Owing to the better inclusion of correlation effects in the wavefunction due to the intra-cluster dynamics, the CGMF method captures the evolution of the dynamical wavefunction in the ‘‘impulse’’ regime of the KZM more accurately. Naturally, in

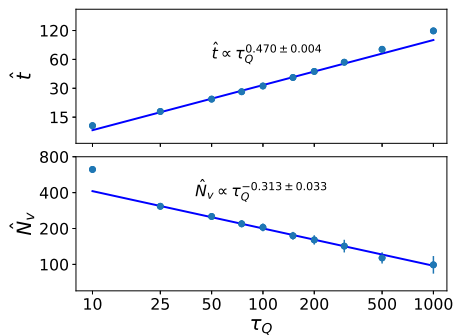


FIG. 8. Power law scaling of \hat{t} and \hat{N}_ν with CGMF using 7-fold growth factor of ϕ as indicator for \hat{t} for cluster size of 2×2 .

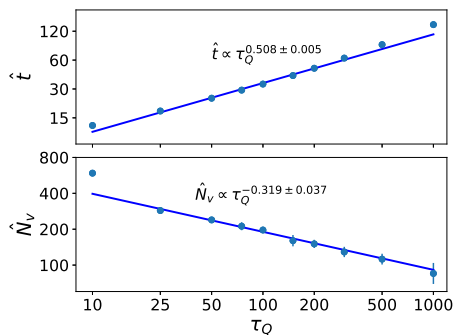


FIG. 9. Power law scaling of \hat{t} and \hat{N}_ν with CGMF using 7-fold growth factor of ϕ as indicator for \hat{t} for cluster sizes 2×3 .

the overlap protocol to determine \hat{t} introduced earlier, the deviation from unity would arise earlier because of the intra-cluster dynamics. This can be seen without ambiguity from the overlap as shown in Fig.7. Thus, the overlap protocol is not suitable for locating the crossover time \hat{t} . The time \hat{t} corresponds to the time at which the SF order parameter develops and inter-cluster dynamics starts. This time can be read from the Fig.6 as the time when the coefficients of the basis states corresponding to an extra particle/hole on top of uniform unit filling (blue color curve) starts growing. This happens at $t \sim 30$ and the SF order parameter around this time grows rapidly compared to its value at criticality as can be seen from the inset of Fig.7.

Motivated by the SGMF studies, we use the definition of 7-fold growth in ϕ as an identifier of \hat{t} to investigate the KZM scaling laws with the CGMF method. The crossover time and defect density show power law scaling with the quench rate as shown in Fig.8 and Fig.9 for CGMF with 2×2 and 2×3 clusters respectively. As can be seen, the power law behaviour deviates for very fast and very slow quenches. The power law scaling is thus evident in the regime $\tau_Q \in [25, 300]$. It is to be noted that a different choice of the growth factor $\phi(\hat{t})/\phi(0)$ for locating crossover time leads to different scaling exponents similar to the SGMF case as shown in Fig.10. Using the KZ scaling laws $\hat{t} \propto (\tau_Q)^{\frac{\nu}{1+\nu z}}$, and $\hat{N}_\nu \propto (\tau_Q)^{-\frac{\nu}{1+\nu z}}$, we obtain the critical exponents ν and z . A comparison of the critical exponents obtained with the SGMF and CGMF meth-

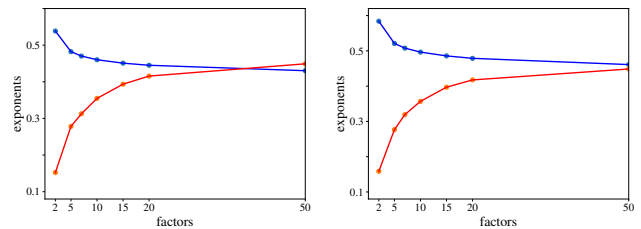


FIG. 10. Scaling exponents for \hat{t} (blue) and \hat{N}_ν (red) for various choices of the growth factor $\phi(\hat{t})/\phi(0)$ with CGMF of cluster 2×2 (left) and 2×3 (right).

cluster	1×1	2×2	2×3
$\frac{\nu z}{1+\nu z}$	0.484 ± 0.003	0.470 ± 0.004	0.508 ± 0.005
$\frac{\nu}{1+\nu z}$	0.347 ± 0.034	0.313 ± 0.033	0.319 ± 0.037
z	1.39 ± 0.15	1.50 ± 0.17	1.59 ± 0.20
ν	0.67 ± 0.09	0.59 ± 0.09	0.65 ± 0.11

TABLE I. Critical exponent for \hat{t} and \hat{N}_ν for various cluster sizes, for QPT at $\mu = 0.3$.

ods for 7-fold growth in ϕ as a locator for \hat{t} is shown in Table I where 1×1 cluster means the SGMF method. The critical exponent ν , which is associated with the divergence of the correlation length (ξ), shows a marginal change with the SGMF and CGMF method but doesn't show any trend with the cluster sizes. However the critical exponent z , which is associated with the divergence of the relaxation time (τ), shows an increasing trend with the increase in the cluster size. These calculated exponents can be compared with the equilibrium mean-field exponents $\nu = 1/2$ and $z = 2$.

B. Quench across the tip of MI(1) lobe

We quench the initial MI state across the multi-critical point at the tip of the MI(1) lobe ($\mu = 0.4$). This continuous QPT corresponds to the 3D XY model universality class. As described earlier, the initial state corresponds to the equilibrium MI(1) state and is dressed with random fluctuations. The dressed state is then time evolved by quenching J across the QPT into the SF regime. Similar to the previously discussed case of quantum quench below the tip of the Mott lobe ($\mu = 0.3$), we observe a delayed growth of the average SF order parameter in the quenched state. And the quenched state has topological defects (vortex-antivortex pairs). With the SGMF method, we find impulse regime near the criticality and thus utilize the overlap protocol for the identification of crossover time \hat{t} . We observe power law behaviour of the cross-over time $\hat{t} \propto \tau_Q^{0.421 \pm 0.004}$ and the defect density $\hat{N}_\nu \propto \tau_Q^{-0.325 \pm 0.036}$ and is shown in Fig.11. The power law fitting is done using data in the regime $\tau_Q \in [25, 300]$. We also observe that the overlap protocol for locating \hat{t} is consistent with the 7-fold growth in ϕ compared to the value at criticality. The power-law exponents are different from the previ-

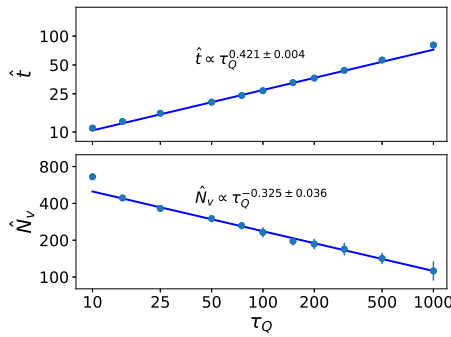


FIG. 11. Power law scaling of \hat{t} and \hat{N}_v , calculated with SGMF using the overlap criterion for locating \hat{t} .

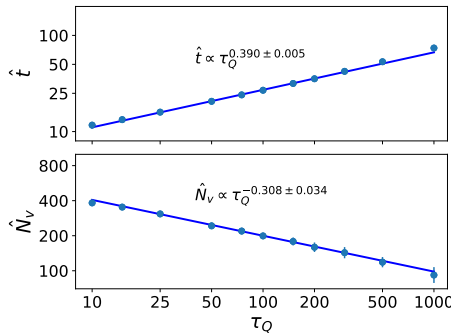


FIG. 12. Power law scaling of \hat{t} and \hat{N}_v , with 2×2 cluster

ously obtained exponents at $\mu = 0.3U$. This is expected since the QPT at the tip belongs to a different universality class with the critical exponents given by the 3D XY model. From the power law exponents of cross-over time and the defect density, we find $\nu = 0.56 \pm 0.09$ and $z = 1.30 \pm 0.16$ which should be compared with the equilibrium values $\nu = 2/3$ and $z = 1$.

With CGMF we use 2×2 and 2×3 clusters to study the evolution of the quenched state across the QPT. As seen previously for QPT at $\mu = 0.3$, we observe that the dynamical state evolves in the “impulse regime”. Utilizing the 7-fold growth in ϕ as locator for crossover time, the power law scalings for cross-over time and defect density are shown in Fig.12 and Fig.13 for CGMF studies with 2×2 and 2×3 cluster respectively. A comparison of the critical exponents with SGMF and CGMF methods, obtained using the 7-fold growth in ϕ for locating \hat{t} is shown in Table II. The results suggests the critical exponents $\nu \sim 1/2$ and $z \sim 1$ which are close to the equilibrium critical exponents for 3D XY model $\nu = 2/3$ and $z = 1$.

IV. CONCLUSIONS

We have studied the quantum quench dynamics of ultra-cold bosons in a 2D square optical lattice. The quenching of hopping amplitude drives the QPT across the MI-SF phase

boundary of BHM. We study the dynamical properties of the quenched state from the perspective of KZM and have ob-

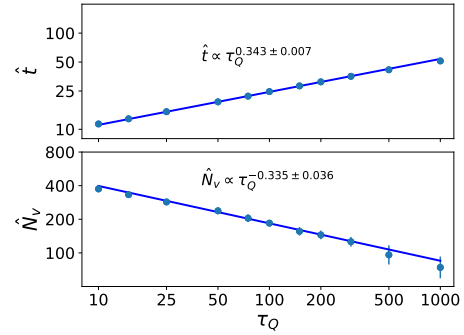


FIG. 13. Power law scaling of \hat{t} and \hat{N}_v , with 2×3 cluster

cluster	1×1	2×2	2×3
$\frac{\nu z}{1+\nu z}$	0.407 ± 0.004	0.390 ± 0.005	0.343 ± 0.007
$\frac{\nu}{1+\nu z}$	0.335 ± 0.032	0.308 ± 0.034	0.335 ± 0.036
z	1.21 ± 0.13	1.27 ± 0.16	1.02 ± 0.13
ν	0.57 ± 0.08	0.50 ± 0.09	0.51 ± 0.10

TABLE II. Critical exponent for \hat{t} and \hat{N}_v for various cluster sizes, for QPT at $\mu = 0.4$.

tained the power-law scaling of the crossover time and defect density with the quench rate using the SGMF and CGMF methods. The power-law behavior, however, deviates at very slow and fast quenches. The CGMF studies capture the evolution of the quenched state in the “impulse” regime of the KZM. The critical exponents obtained from the dynamics are close to the equilibrium values. In particular, the critical exponent z , which is associated with the divergence of the relaxation time, improves towards the equilibrium value with higher cluster sizes of CGMF. This is expected as the larger cluster size allows a large number of basis states for redistribution of the population in the initial state and allows better relaxation dynamics.

V. ACKNOWLEDGEMENTS

The results presented in this paper were computed on Vikram-100, the 100TFLOP HPC cluster and Param Vikram-1000 HPC cluster at Physical Research laboratory, Ahmedabad, India. DA would like to acknowledge support from the Science and Engineering Research Board, Department of Science and Technology, Government of India through Project No. CRG/2022/007099 and support from the UGC through the SAP (DRS-II) project F.530/18/DRS-II/2018(SAP-I), Department of Physics, Manipur University. The authors are grateful to Dr. Sukla Pal, Dr. Kuldeep Suthar, Dr. Rukmani Bai and Dr. Soumik Bandyopadhyay for the fruitful discussions.

- [1] W. H. Zurek, “Cosmological experiments in superfluid helium?” *Nature* **317**, 505 (1985).
- [2] Wojciech H. Zurek, Uwe Dorner, and Peter Zoller, “Dynamics of a quantum phase transition,” *Phys. Rev. Lett.* **95**, 105701 (2005).
- [3] Jacek Dziarmaga, “Dynamics of a quantum phase transition: Exact solution of the quantum ising model,” *Phys. Rev. Lett.* **95**, 245701 (2005).
- [4] Adolfo del Campo and Wojciech H. Zurek, “Universality of phase transition dynamics: Topological defects from symmetry breaking,” *International Journal of Modern Physics A* **29**, 1430018 (2014).
- [5] W.H. Zurek, “Cosmological experiments in condensed matter systems,” *Physics Reports* **276**, 177 (1996).
- [6] V. M. H. Ruutu, V. B. Eltsov, A. J. Gill, T. W. B. Kibble, M. Krusius, Yu. G. Makhlin, B. Plaçais, G. E. Volovik, and Wen Xu, “Vortex formation in neutron-irradiated superfluid ^3He as an analogue of cosmological defect formation,” *Nature* **382**, 334 (1996).
- [7] C. Bäuerle, Yu. M. Bunkov, S. N. Fisher, H. Godfrin, and G. R. Pickett, “Laboratory simulation of cosmic string formation in the early universe using superfluid ^3He ,” *Nature* **382**, 332 (1996).
- [8] Jacek Dziarmaga, Marek Tylutki, and Wojciech H. Zurek, “Quench from mott insulator to superfluid,” *Phys. Rev. B* **86**, 144521 (2012).
- [9] M. Lewenstein, A. Sanpera, V. Ahufinger, B. Damski, A. Sen(De), and U. Sen, “Ultracold atomic gases in optical lattices: mimicking condensed matter physics and beyond,” *Adv. Phys.* **56**, 243 (2007).
- [10] Christian Gross and Immanuel Bloch, “Quantum simulations with ultracold atoms in optical lattices,” *Science* **357**, 995 (2017).
- [11] M. P. A. Fisher, P. B. Weichman, G. Grinstein, and D. S. Fisher, “Boson localization and the superfluid-insulator transition,” *Phys. Rev. B* **40**, 546 (1989).
- [12] D. Jaksch, C. Bruder, J. I. Cirac, C. W. Gardiner, and P. Zoller, “Cold bosonic atoms in optical lattices,” *Phys. Rev. Lett.* **81**, 3108 (1998).
- [13] M. Greiner, O. Mandel, T. Esslinger, T. W. Hänsch, and I. Bloch, “Quantum phase transition from a superfluid to a Mott insulator in a gas of ultracold atoms,” *Nature (London)* **415**, 39 (2002).
- [14] Markus Greiner, Olaf Mandel, Theodor W. Hänsch, and Immanuel Bloch, “Collapse and revival of the matter wave field of a bose-einstein condensate,” *Nature* **419**, 51 (2002).
- [15] David Chen, Matthew White, Cecilia Borries, and Brian DeMarco, “Quantum quench of an atomic mott insulator,” *Phys. Rev. Lett.* **106**, 235304 (2011).
- [16] Simon Braun, Mathis Friesdorf, Sean S. Hodgman, Michael Schreiber, Jens Philipp Ronzheimer, Arnau Riera, Marco del Rey, Immanuel Bloch, Jens Eisert, and Ulrich Schneider, “Emergence of coherence and the dynamics of quantum phase transitions,” *Proceedings of the National Academy of Sciences* **112**, 3641 (2015).
- [17] Werner Weiss, Matthias Gerster, Daniel Jaschke, Pietro Silvi, and Simone Montangero, “Kibble-zurek scaling of the one-dimensional bose-hubbard model at finite temperatures,” *Phys. Rev. A* **98**, 063601 (2018).
- [18] Keita Shimizu, Yoshihito Kuno, Takahiro Hirano, and Ikuo Ichinose, “Dynamics of a quantum phase transition in the bose-hubbard model: Kibble-zurek mechanism and beyond,” *Phys. Rev. A* **97**, 033626 (2018).
- [19] Keita Shimizu, Takahiro Hirano, Jonghoon Park, Yoshihito Kuno, and Ikuo Ichinose, “Out-of-equilibrium dynamics of multiple second-order quantum phase transitions in an extended bose-hubbard model: Superfluid, supersolid, and density wave,” *Phys. Rev. A* **98**, 063603 (2018).
- [20] Keita Shimizu, Takahiro Hirano, Jonghoon Park, Yoshihito Kuno, and Ikuo Ichinose, “Dynamics of first-order quantum phase transitions in extended bose-hubbard model: from density wave to superfluid and vice versa,” *New Journal of Physics* **20**, 083006 (2018).
- [21] Yijia Zhou, Yongqiang Li, Rejish Nath, and Weibin Li, “Quench dynamics of rydberg-dressed bosons on two-dimensional square lattices,” *Phys. Rev. A* **101**, 013427 (2020).
- [22] Hrushikesh Sable, Deepak Gaur, Soumik Bandyopadhyay, Rejish Nath, and Dilip Angom, “Quantum quench dynamics of tilted dipolar bosons in 2d optical lattices,” *arXiv:2106.01725v2* (2021), *arXiv:2106.01725v2*.
- [23] Hrushikesh Sable, Deepak Gaur, and D. Angom, “Fine-grained domain counting and percolation analysis in 2d lattice systems with linked-lists,” *arXiv:2112.15527* (2021), *arXiv:2112.15527*.
- [24] Pardeep kaur, Kuldeep Suthar, D. Angom, and Sandeep Gautam, “Out-of-equilibrium dynamics of bose-bose mixtures in optical lattices,” *arXiv:2307.13057* (2023), *arXiv:2307.13057v1*.
- [25] Giulio Biroli, Leticia F. Cugliandolo, and Alberto Sicilia, “Kibble-zurek mechanism and infinitely slow annealing through critical points,” *Phys. Rev. E* **81**, 050101 (2010).
- [26] Kangeun Jeong, Bongsoo Kim, and Sung Jong Lee, “Growth kinetics of the two-dimensional ising model with finite cooling rates,” *Phys. Rev. E* **99**, 022113 (2019).
- [27] Krishanu Roychowdhury, Roderich Moessner, and Arnab Das, “Dynamics and correlations at a quantum phase transition beyond kibble-zurek,” *Phys. Rev. B* **104**, 014406 (2021).
- [28] Anatoli Polkovnikov, Krishnendu Sengupta, Alessandro Silva, and Mukund Vengalattore, “Colloquium: Nonequilibrium dynamics of closed interacting quantum systems,” *Rev. Mod. Phys.* **83**, 863–883 (2011).
- [29] Dmitry A. Abanin, Ehud Altman, Immanuel Bloch, and Maksym Serbyn, “Colloquium: Many-body localization, thermalization, and entanglement,” *Rev. Mod. Phys.* **91**, 021001 (2019).
- [30] D. S. Rokhsar and B. G. Kotliar, “Gutzwiller projection for bosons,” *Phys. Rev. B* **44**, 10328 (1991).
- [31] K. Sheshadri, H. R. Krishnamurthy, R. Pandit, and T. V. Ramakrishnan, “Superfluid and insulating phases in an interacting-boson model: Mean-field theory and the RPA,” *EPL* **22**, 257 (1993).
- [32] D.-S. Lühmann, “Cluster Gutzwiller method for bosonic lattice systems,” *Phys. Rev. A* **87**, 043619 (2013).
- [33] Soumik Bandyopadhyay, Rukmani Bai, Sukla Pal, K. Suthar, Rejish Nath, and D. Angom, “Quantum phases of canted dipolar bosons in a two-dimensional square optical lattice,” *Phys. Rev. A* **100**, 053623 (2019).
- [34] R. Bai, S. Bandyopadhyay, S. Pal, K. Suthar, and D. Angom, “Bosonic quantum Hall states in single-layer two-dimensional optical lattices,” *Phys. Rev. A* **98**, 023606 (2018).